

## Differential Modal Delay Measurements in a Graded-Index Multimode Fibre Optical Waveguide, Using a Single-mode Fibre for Mode Selection

HARISH R. D. SUNAK and SONIA MARIA SOARES

*Instituto de Física, Universidade Estadual de Campinas, 13100 Campinas, SP*

Recebido em 16 de Fevereiro de 1981

We have carried out differential modal delay (DMD) measurements in graded-index multimode optical fibre waveguides, which are very promising for many types of communication systems. These DMD measurements give a direct indication of the deviation of the refractive index profile, from the optimum value, at a given wavelength. For the first time, by using a single-mode fibre, we selected a few guided modes in the graded-index fibre, in two different ways: launching a few modes at the input end or selecting a few modes at the output end. By doing so, we have revealed important features of propagation in the fibre, especially the intermodal coupling that may exist. We discuss (1) the importance of this determination of intermodal coupling or mode mixing, particularly when many fibres are joined together in a link, and (2) the merits of DMD measurements in general and their importance for the production of high bandwidth graded-index fibres.

Concluimos medidas de atraso diferencial de modos (DMD) em fibras ópticas multimodo de índice graduado, as quais são muito promissoras para vários tipos de sistemas de comunicações. Estas medidas DMD dão uma indicação direta do desvio do perfil de índice de refração de um valor ótimo, em um determinado comprimento de onda. Pela primeira vez, usando-se uma fibra monomodo, selecionamos poucos modos guiados na fibra de índice graduado, de duas maneiras diferentes: lançando poucos modos na entrada ou selecionando poucos modos na saída. Fazendo isto, temos revelado aspectos importantes da propagação na fibra, especialmente o acoplamento intermodal que possa existir. Nós discutimos (1) a importância

desta determinação do acoplamento intermodal ou mistura dos modos, particularmente quando há conexão de muitas fibras em um sistema, e (2) os méritos destas medidas em geral e sua importância para a produção de fibras de índice graduado com grande largura de banda.

## 1. INTRODUCTION

There are three basic fibre types<sup>1,2</sup> for use in different types of fibre optical communication systems<sup>2</sup>. By using highly pure silica and other raw materials, the attenuation in these fibres has been reduced to very small values ( $\leq 1$  db/km) close to the limit imposed by Rayleigh scattering. Hence a considerable amount of attention is now being given to the bandwidth and other systems considerations. A multimode step-index fibre has large intermodal dispersion<sup>1</sup> (50 nsec/km for every percent of refractive index difference between core and cladding) and hence the bandwidth is limited to a few megahertz per kilometre; however the core diameter of  $\approx 50\mu\text{m}$  allows (i) power coupling from cheap and reliable light emitting diodes (LED) and (ii) fabrication of very low-loss splices and connectors. Intermodal dispersion is eliminated by designing a single-mode fibre, in which the intramodal<sup>1</sup> or material dispersion limits the bandwidth. Since this dispersion is fairly small and goes to zero in the region  $1,3\mu\text{m}$  to  $1,6\mu\text{m}$ , depending on the fibre material composition and geometry, bandwidths of many tens of gigahertz over tens of kilometers are possible. However, since the core diameter is fairly small,  $\approx 5\mu\text{m}$ , the fabrication of low-loss splices and connectors is a fairly difficult problem, and semiconductor lasers have to be used for mode launching. A graded-index multimode fibre incorporates the advantages of the two fibre types discussed above, namely, core diameters  $\approx 50\mu\text{m}$  and much smaller intermodal dispersion and hence considerably larger bandwidths, especially when operated in the zero material dispersion region, even with LED excitation.

In a graded-index multimode fibre, the refractive index decreases radially from  $n_1$ , at the core axis, towards the core/cladding boundary, approximately as follows<sup>3,4</sup>:

$$n(r) = n_1 \left[ 1 - 2\Delta \left( \frac{r}{a} \right)^{\alpha} \right]^{1/2}; \quad r < a \quad (1)$$

$$n(r) = n_1 [1 - 2\Delta]^{1/2} = n_2; r \geq a \quad (2)$$

where  $a$  is the core radius,  $n_2$  is the cladding index and  $\Delta$  is constant for  $r > a$ ,  $r$  is the distance from the fibre axis,  $\alpha$  is a power law exponent that characterizes the refractive index profile, and  $A$  is the relative index difference between the core centre and cladding, and is given by

$$A = (n_1^2 - n_2^2)/2n_1^2 \quad (3)$$

$$\approx (n_1 - n_2)/n_1$$

The rays in a step-index fibre follow zigzag paths in the core, while those in a graded-index fibre follows quasi-sinusoidal paths<sup>1</sup>. The optimum profile,  $\alpha_{opt}$ , at a particular wavelength, is one for which the group velocity variation from ray to ray most nearly compensates the corresponding path length variation. When  $\alpha > \alpha_{opt}$ , the profile is said to be undercompensated, i.e., off-axis rays arrive later than the ray that has the shortest pathlength along the fibre axis. On the other hand, with  $\alpha < \alpha_{opt}$  the profile is overcompensated, i.e., the axial ray arrives last because the refractive-index gradient decreases so rapidly towards the core/cladding interface that the longer propagation lengths of the off-axis rays are overcompensated by their fast speeds. Hence the output shapes in each case will be different, when the fibre is excited with a short pulse. With  $\alpha > \alpha_{opt}$ , the leading edge will be short and the trailing edge will be much longer; whereas for  $\alpha < \alpha_{opt}$  the leading edge will have a longer duration than the trailing edge of the output pulse. This will only be observed in fibres with very small amounts of mode mixing, as each ray will retain its propagation time. The reader is referred to fig. 4 in Cohen's paper<sup>5</sup> for illustration of these effects in many kilometers of fibre. The presence of strong mode mixing would lead to an averaging of the propagation times.

With  $\alpha_{opt}$ , theory predicts reductions in intermodal dispersion by as much as several orders of magnitude<sup>3,4</sup> from what it would be in a step-index multimode fibre, which effectively has  $\alpha = \infty$ . Now  $\alpha_{opt}$  is wavelength dependent, and its value differs from 2 because dispersive refractive index difference between the materials<sup>2</sup> that make the fibre (e. g.  $B_2O_3$  and  $SiO_2$  for borosilicate fibres) causes modal group velocities

to depend not only on the index profile but also on the wavelength; this is called profile dispersion<sup>3</sup>.

The predicted large reduction of intermodal dispersion has been difficult to achieve in practice because  $a_{opt}$  is very critical; a small departure of  $a$  from  $a_{opt}$ , say for example that  $a = a_{opt} (1 \pm \Delta)$ , would increase the intermodal dispersion by an order of magnitude. Measuring this total dispersion, by comparing the duration of a subnanosecond pulse before and after propagation in such a fibre, does not give quantitative data as to the radial position where the profile deviates from its optimum value. Qualitative estimates, as to whether the profile is overcompensated or undercompensated, can be made by observing the output pulse shapes, with the elimination of either near-axis or off-axis rays with apertures or annular rings<sup>5</sup>.

Quantitative data can be obtained (i) directly by measuring the refractive index profile with the various interferometric and other techniques available<sup>2</sup>, or (ii) indirectly by carrying out the so-called differential modal delay (DMD) measurements on the fibres. These latter measurements, first made by Jeunhomme and Pacholle<sup>6</sup>, are done by measuring the pulse propagation times of the various propagating modes, after launching a few modes at a time along the radial position, from  $(r/a)=0$  to  $-1$ , i.e., varying the mode number. Deviations from the optimum index profile shows up directly as differences in the propagation time. Such DMD measurements are gaining considerable importance because they can be used directly in a feedback loop, to modify the dopant gas flows for the preform deposition layers and hence minimising the DMD time in successively manufactured preforms. The bandwidth increases as DMD becomes more constant and of a lower magnitude. In a fiber with  $a_{opt}$ , no difference in the propagation time will be observed as the excitation of a few modes is progressively carried out from the core axis ( $r/a=0$ ) towards the core/cladding interface ( $r/a = 1$ ). Hence DMD measurements<sup>7-14</sup> have considerable importance as measurements made on the fibre itself are directly used to improve<sup>12,13</sup> the bandwidth of the subsequently produced fibres. The technique will obviously not be useful in fibers with strong mode coupling as an averaging of the propagation times will occur; however, well-made present day fibres have very small mode coupling over many kilometers and any wrapping tension, which causes mode coupling due

to microbending, can be eliminated by using a metallic drum, on which the fibre can be wound, and then cooling this drum.

Apart from this nominal disadvantage, there are many other **careful** advantages<sup>7</sup> for using **DMD** measurements to determine deviations of the refractive index from  $\alpha_{opt}$ , rather than by direct measurement of the profile using various interferometric techniques<sup>2</sup>. These are as follows: (1) A minimum of fibre preparation is required as both ends of the fibres need to be broken flat and perpendicular to the fibre axis to within  $<1^\circ$ . For direct measurement, time-consuming careful preparation of a thin transverse slice is required, involving grinding and polishing, so that the ends be flat and parallel; (2) An average of the profile over the entire length of the fibre is obtained as azimuthal profile variation or length-dependence is automatically averaged; whereas in the direct measurement, only a very thin sample is measured and the assumption is then made that the profile is similar over the whole fiber length; the presence of mode coupling will render this assumption invalid. (3) **DMD** measurement do not suffer from systematic uncertainties as other direct measurement methods do; (4) **DMD** measurements are very sensitive to small profile changes; a **DMD** time of 0,1 nsec/km, which is easy to measure, corresponds to difference of  $\sim 0,01$  in the  $\alpha$  value. Hence, very small index differences can be measured, this being difficult in direct measurements; (5) The data can be gathered very rapidly and can also be interpreted directly<sup>7</sup> as the **DMD** measures the difference between the actual and optimum profile; hence the need for precise curve fitting is avoided as needed in direct measurements. Further in these latter measurements, analysis of typical refractive index data encounters ambiguities, such as the proper weighting for the on-axis index perturbation, the rounding of the profile at the core/cladding interface, or the choice of an overall weighting function. In a practical situation, these ambiguities make it difficult to determine small refractive index perturbations. **DMD** measurements avoids all these difficulties and further, even makes a knowledge of  $\alpha_{opt}$  unnecessary; (6) **DMD** measurements can be used in a production environment as they are very similar to other quality control measurements. This has already been demonstrated by Buckler<sup>13</sup> and will be discussed further later. (7) In the laboratory, **DMD** measurements can be carried out with the same laser type as would be used in a system; hence

$a_{opt}$  can be obtained at the exact wavelength, without any need for extrapolation using different profile measurements.

It is clear that DMD measurements are of considerable importance due to their many advantages, but relatively few reports<sup>7-14</sup> of these exist in the literature. In view of these facts, we are also carrying out a detailed and systematic study of DMD measurements and this paper reports the initial results obtained. We shall discuss and compare our measurement techniques and results with those used by other researchers. We shall also discuss their importance for optimum system design when many fibres are linked together.

## 2. SELECTION OF A FEW GUIDED MODES

The selection of a few guided mode in a graded-index fibre can be made by two methods: (1) launching a few modes at the input end, or (2) selecting a few modes at the output end of the fibre with all modes launched at the input end.

Launching a few modes at the input end is fairly easy from lasers operating in the fundamental TEM<sub>00</sub> Gaussian spatial mode and giving collimated beams. Jeunhomme et al.<sup>6,8</sup> used a mode-locked Nd: YAG laser and Olshansky and Oaks<sup>7</sup> used a mode-locked Krypton-ion laser. The only important point is the selection of the lens which will focus the output beam from the laser onto the fibre input end, where the optimum launching radius ( $\omega_0^l$ ) at the  $(1/e^2)$  times maximum intensity points, is given by<sup>6</sup>

$$\omega_0^l = \left(\frac{\lambda}{\pi}\right)^{1/2} \left(\frac{\alpha^2}{2\Delta}\right)^{1/4} \quad (4)$$

This is a tradeoff condition for launching a few modes where the natural tendency of the input beam to spread is counterbalanced by the refractive index variation. It comes about from a practical point of view since with  $\omega_0^l \rightarrow 0$ , the divergence will be infinite and all modes will be launched. On the other extreme, as  $\omega_0^l \rightarrow \infty$ , there will be no divergence, but again all modes will be launched. Equation (4) gives the best trade-off between these two extremes. As an example, with  $\lambda=0,85\mu\text{m}$ ,  $\alpha=28\mu\text{m}$ ,  $\Delta=0,0064$ ,

$\omega_0' = 8,2 \mu\text{m}$ . Knowing this value of  $\omega_0'$  and the corresponding value ( $\omega_z'$ ) of the beam at the position of the launching lens, the focal length ( $f$ ) of this lens can easily be calculated from

$$\tan \theta \approx \theta = \frac{\omega_z'}{f} = \frac{\lambda}{\pi \omega_0'} \quad (5)$$

The output beams from semiconductor diode lasers are highly divergent and not circularly symmetric. Hence to launch a few modes using these lasers, the output beam has first to be collimated using a x20 microscope objective, then apertured spatially before achieving the condition of equation (4) at the fibre input end, as done by Jeunhomme et al.<sup>8,11</sup>.

As already mentioned, measurements performed with semiconductor lasers have great importance since these are being used in practical systems and if the same laser type is used for the measurements, no extrapolation of the  $\alpha_{\text{opt}}$  value is required. The above techniques using microscope objectives and apertures are cumbersome. Buckler<sup>12-14</sup> has used a single-mode fibre, butt-coupled to the test graded-index fibre, to launch a few modes. Since this technique is fairly simple and avoids complicated beam optics, we have adopted this technique for exciting a few modes of the graded-index fibre we tested. The single-mode fibre can be selected so that the near-field intensity distribution approximately satisfies the condition in Equation (4).

For selecting a few modes at the output end of the fibre, the first important consideration is the launching of all modes at the input end. This can be achieved<sup>10</sup> by using a mode scrambling fibre and butt-coupling it onto the test fibre; then selection of modes can be accomplished by using<sup>10</sup> beam optics and annular rings. Again, we consider that this technique is fairly cumbersome and have extended Buckler's<sup>12</sup> technique to the output end, i.e. we have also used a single-mode to select a few modes at the output end. It is the first time that such selection of a few guided modes in a graded-index fibre, at both ends of the fibre, has been accomplished. By doing so, we have established a new and simple technique for directly determining the presence of mode coupling in the fibre at the test wavelength. The technique can be used routinely on a quality control basis to directly determine the extent of mode conversion in the fibre.

### 3. DMD MEASUREMENT SYSTEM

The experimental set-up for DMD measurements is shown in Fig.1. The laser L is a semiconductor laser made by Laser Diode Laboratories in the U.S.A., and is of the type designated LA-60. It has a peak output wavelength of 880nm, with a spectral bandwidth of approximately 2nm, and is driven by a simple electronic circuit to produce pulses with a duration of ~100 psec, having peak powers of many hundreds of milliwatts, at a repetition rate of ~1 kHz. Using an Ealing tetravar unit T1, the output from the laser is first collimated using a high numerical aperture (0.54) x20 microscope objective M1, as the light from the semiconductor laser is highly divergent. The beam-splitter in T1 splits the collimated light into two paths: (i) microscope objective M2, x10 launches part of this light into a single-mode fibre (SMF) having a nominal core diameter of 8  $\mu\text{m}$ , and (ii) microscope objective M3, x10, launches the other part of the light into a fibre delay line; the need for this is discussed further below.

Our SMF has  $\omega_0^1 = 5.2 \mu\text{m}$  compared to an optimum value of 8.2  $\mu\text{m}$  for our test fibre and is the nearest value that could be obtained, due to the non-availability of an optimum SMF. We measured the far-field pattern from the fibre with a Reticon scanning photodiode array (SPA) and the gaussian spatial profile of the  $\text{HE}_{11}$  fundamental mode is shown in fig.2. The fibre was excited by a cw semiconductor laser operating at 850 nm and was necessary to give a high average power for detection by the SPA. The distance between the fibre end and the SPA is 61mm, and the full width of SPA, as in fig. 2, is 27mm. We also confirmed the above value of  $\omega_0^1$  by measuring the fibre output angular spatial distribution with a pin-hole and obtained a divergence of  $4.2^\circ$ , to the 1/e times maximum intensity points. .

The SMF is butt-coupled to the graded-index fibre (GIF) which is to be tested. Butt-coupling implies axial separation of a few microns between the two fibre ends. The SMF has ~2m length and its output end is fixed, while the input end of GIF is held in a precision micromanipulator (PMM), which gives a remotely controlled positional accuracy of 0.4  $\mu\text{m}$  in the radial scanning direction ( $x$ ), i.e., perpendicular to the fibre axis. Great care is taken to break the ends of the SMF and the EIF,



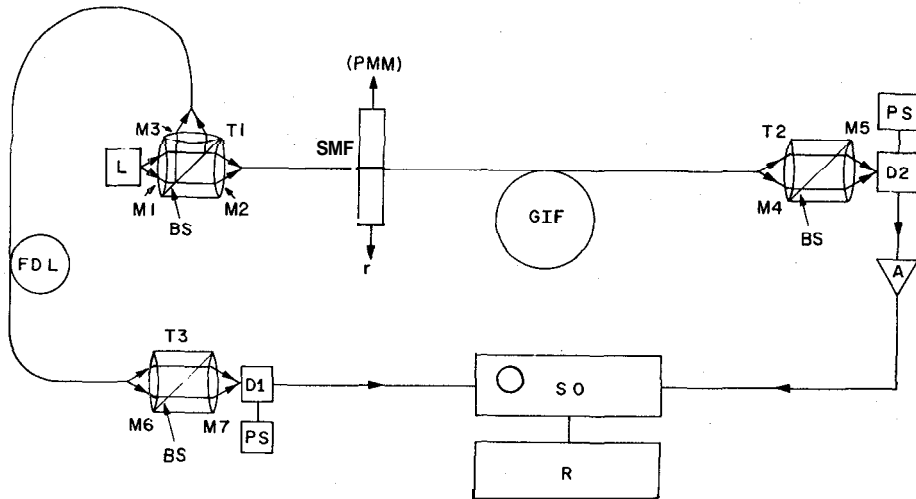


Fig.1 - Experimental set-up used for differential modal delay measurements. M1 to M7 - Microscope objectives; L - pulsed Semiconductor Laser; T1 to T3 - Ealing Tetravar units; BS - Beam Splitter; D1 and D2 - silicon avalanche detectors; A - wide bandwidth preamplifier; SMF - Single mode fibre; GIF - grade-index fibre under test; RM - precision micromanipulator; PS - power supply for detectors; FDL - fibre delay line; SO - Sampling Oscilloscope; R - x-y recorder.

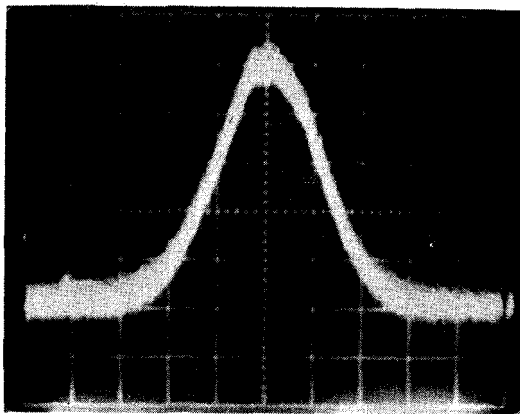


Fig.2 - Far-field spatial intensity distribution of the fundamental mode of the single-mode fibre, measured 61 mm from the fibre end, with a Reticon scanning photodiode array.

so that the broken ends are perpendicular to the fibre axis to within  $1^\circ$ . Using the SMF in this way, we select a few modes of the GIF at its input end. Selection of a few modes at the output end of the GIF is accomplished by (i) launching all modes into the GIF with M2 and also using a

mode scrambler soon after launch, (ii) placing the output end of the GIF on the PM, and then butt-coupling the SMF to this end.

Another tetravar unit T2 is used at the output end of the GIF, as shown in fig. 1 (with mode selection at the output end of the GIF, T2 is used at the output end of the SMF). The output pulses from the fibre are detected by D2, a silicon avalanche photodiode (ADP), made by Optel, Model 103, and subsequently amplified by a wide bandwidth pre-amplifier (HP 8774D). The output pulses are displayed on a sampling oscilloscope (Philips Model RM 3400). Very stable, and jitter-free, external triggering of the oscilloscope is fundamental in DMD measurements so that very small time differences can be resolved clearly as the mode number is increased. For a one kilometer length of GIF, the total propagation time of the pulse is  $\sim 5\mu\text{sec}$ ; hence the trigger pulse to the oscilloscope also has to be delayed by this time interval from the beam-splitter of T1. A digital delay generator (e.g. HP 5359A Time Synthesizer) can be used<sup>12-14</sup> to generate this high delay with an extremely small jitter of  $\pm 10$  ps rms. Buckler, of Bell Labs., has said, in a private communication, that this is an actually measured jitter in the particular time Synthesizer he used; the manufacturer quote a typical jitter of 100 ps rms. A high jitter in this range would be unacceptable in our present measurements as the maximum DMD time was  $\sim 300$  ps. Due to the non-availability of a suitable delay generator, we used a fibre delay line; part of the light from the laser is launched into the delay line with MB and detector D1 provides the external electrical trigger pulse to the oscilloscope. The length of the fibre delay line is slightly shorter than the GIF under test. In this way, very stable and effectively jitter-free triggering of the oscilloscope is achieved, enabling a DMD time of a few tens of picoseconds, in the pulse peaks, to be easily resolved. The pulses on the sampling oscilloscope are recorded on a X-Y recorder.

In both types of mode selection, we immersed many centimeters of the SMF, both at its input and output ends, in index-matching liquid (IML), having refractive index higher than the cladding. We did this so as to be sure that the light launched and propagating in the cladding of the SMF is completely stripped away. If this is not done, a smooth output profile of the spatial propagating mode will not be observed, as shown in fig. 3 (a). With the IML this will not happen, as shown in fig. 3 (b). We found

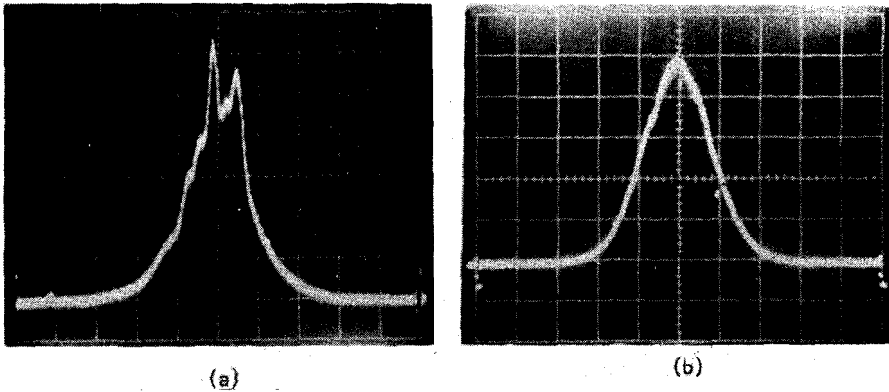


Fig.3 - Effect of index-matching liquid (IML) for cladding modes stripping in the single-mode fibre (a) without IML; (b) with IML near the output end of the single-mode fibre.

that it was more important to put IML at the output end of the SMF than at its input end, where the light is launched.

The test GIF used in our DMD measurements was made at the laboratories of Bell-Northern Research (BNR), in Ottawa, Canada. The fibre, designated as n? 417, had a length of one kilometre, with a secondary protective coating, and an attenuation of 3 dB/km at 840 nm. The nominal numerical aperture was 0,16, nominal core diameter 60µm and fibre diameter 125µm. The fibre delay line was made up of two fibres joined together to give a length of just less than one kilometre.

#### 4. RESULTS AND DISCUSSION

The BNR test fibre was measured in Ottawa to determine its total dispersion, due to intermodal dispersion and material dispersion. A 2km length was pulled and measured and then a 1 km length was sent to our laboratories for further measurements. The results obtained at BNR and at Unicamp, on these different fibre lengths, are summarized in Table 1. All modes were launched and collected with x10 microscope objectives. The pulse profiles obtained in our laboratories are shown in fig. 4. The input pulse was measured with attenuation so as to give the same amplitude of 30 mV, as measured in the output pulse. The output pulse shapes in both measurements are nearly Gaussian and hence the total dispersion ( $\tau_T$ ) was calculated using  $\tau_T^2 = \tau_2^2 - \tau_1^2$ , where  $\tau_2$  and  $\tau_1$  are the full-widths,

TABLE 1 - Dispersion measurements on a graded-index fibre (Fibre n° 417) fabricated by BNR, Ottawa, Canada.

	Results obtained at BNR, Ottawa, Canada	Results obtained at UNICAMP, Campinas, Brazil
Fibre length (km)	2 km	1 km
Laser Wavelength ( $\lambda$ )	904 nm	880 nm
Input FWHM* ( $\tau_1$ )	0,40 nsec	0,33 nsec (see fig.4a)
Output FWHM ( $\tau_2$ )	1,35 nsec	0,73 nsec (see fig.4b)
Total Dispersion ( $\tau_T$ )	1,29 nsec	0,65 nsec
Total Estimated Material Dispersion ( $\tau_m$ )	0,4 nsec	0,2 nsec
Total Calculated Intermodal Disper- sion ( $\tau_g$ )	1,23 nsec	0,62 nsec
Total Normalised Intermodal Dispersion ( $\tau_g$ )	0,62 nsec/km (linear dependen- ce assumed)	0,62 nsec/km

\* FWHM = Full-width at half-maximum intensity points.

at half-maximum intensity points, of the output and input pulses respectively. The material dispersion ( $\tau_m$ ) was calculated by using the value of  $-100 \text{ ps}/(\text{nm}\cdot\text{km})$ , previously measured<sup>15</sup> in similar  $\text{GeO}_2 - \text{SiO}_2$  fibres, and a spectral width of  $\sim 2\text{nm}$  for the semiconductor laser. The contribution of intermodal dispersion ( $\tau_g$ ) was deconvolved from  $\tau_T$ , again assuming gaussian pulse shapes. We note that the normalised value of  $\tau_g = 0,62 \text{ nsec}/\text{km}$  obtained from the measurements at BNR, assuming linear length dependence of  $\tau_g$ , corresponds exactly to our measured value, as shown in Table 1. We conclude the following from this excellent agreement: (i) the slightly different laser wavelengths has negligible effect on  $\tau_g$ ,

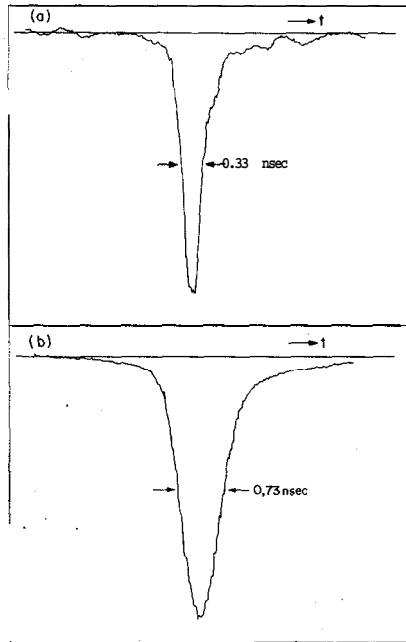


Fig.4 - (a) Input and (b) output pulses to 1 km of BNR graded-index fibre, measured at Unicamp, showing intermodal pulse dispersion of 0,62 nsec/km (see Table 1).

(ii) The gaussian deconvolution is valid as  $\tau_1$  and  $\tau_2$  are very different in each measurement, (iii) most importantly, the linear length dependence of  $\tau_g$  implies that very little mode conversion takes place in the fibre. The DMD results below give more quantitative insight into this initial conclusion and the  $\tau_g$  value will be used for correlation with the 3-dB bandwidth of the fibre, both in our results and those obtained by other researchers. With complete mode mixing in the fibre, a coupling length ( $L_c$ ) will exist, after which  $\tau_g$  will be proportional to  $\sqrt{L}$ .

For our first series of DMD measurements, on the BNR test fibre, we launched a few modes at the input, as shown in fig. 1. The x20 microscope objective M2 collects all the light from the output end and microscope objective M5 (x10) focusses it into detector D<sub>2</sub>. The GIF is scanned in the radial position, across the SMF in 2 $\mu$ m steps, from the centre of the core, with  $(r/a) = 0$ , towards the core/cladding boundary, i.e.  $(r/a) \rightarrow 1$ . At each scan point, the output pulse is recorded on the X-Y recorder and at subsequent radial positions  $(r/a)$ , the pulse is displaced vertically on the recorder so that the pulse shape and the delay of

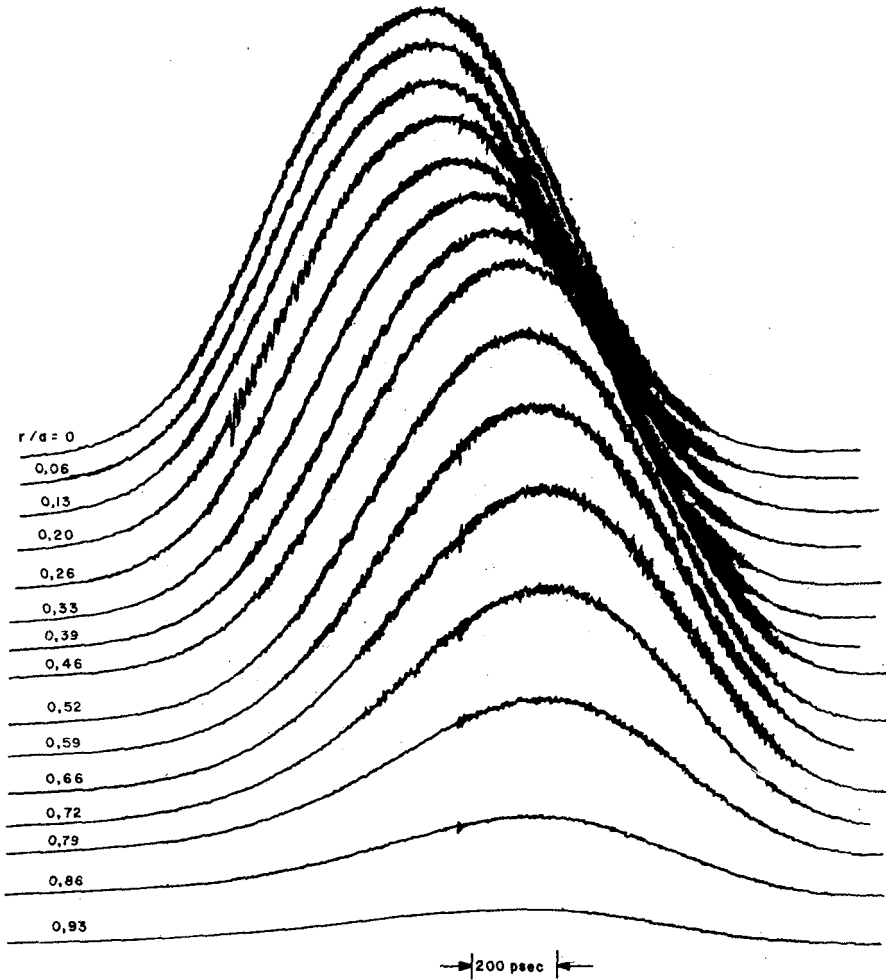


Fig.5 - Output scan obtained as a function of normalised radial position ( $r/a$ ), as shown on the scans: mode selection at the input end of the fibre.

the peak of the pulse, relative to  $(r/a)=0$  pulse, can be accurately determined. The scans are shown in fig.5, the various scans are for different  $(r/a)$ , the radial position,  $a$  being the core radius and  $r$  being the radial displacement. A similar set of scans was obtained for radial displacement in the opposite direction. The DMD time for a scan position on either side of the core axis are averaged to improve the precision of the measurements, and this is plotted in fig. 6 with the dotted line (-----). The actual delays obtained on either side are also shown with

circular points ( $\theta$ ). For clarity, fig. 6 shows DMD time vs  $(r/a)$  on a linear scale. We note that for  $(r/a) < 0,6$ , the measured delay times are completely symmetric to within  $\pm 10$  psec, the measurement error. For  $(r/a) > 0,6$ , the peaks of the pulses are not well defined and hence the measurement error is  $\pm 30$  ps, as indicated by the two error bars on either side of the ordinate axis. Taking this error into consideration, we can conclude that the measured delays are symmetric about the core axis, as would be expected. These measurements are completely repeatable with a new break and also confirm the very stable and jitter-free triggering of the sampling oscilloscope, since -10 minutes are taken for each series of scans, and over this interval of time no delay is observed when the radial launching position is held constant.

The mode group number  $m$  of a near-parabolic graded-index fibre is given as

$$(m/M) \approx (r/a)^2 \tag{6}$$

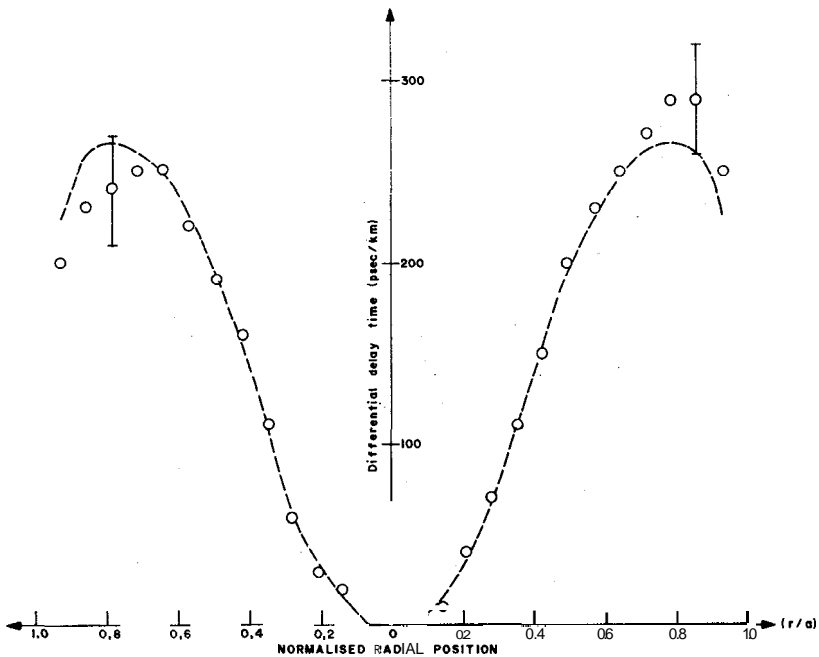


Fig.6 - Differential delay time as a function of normalized radial position  $(r/a)$ , measured at the pulse peaks for mode selection at the input end of the fibre. The points  $\theta$  are experimentally measured points; the dashed line (-----) is the average of the experimental points on either side of  $(r/a) = 0$ .

when  $M$  is the maximum mode number. Hence in fig. 7, we have plotted the results of average DMD time, as obtained in fig. 6, versus mode number  $(m/M)$ . This representation has been mostly used by previous researchers. From fig. 7, we observe that the maximum average DMD time is  $\approx 270$  psec. The bandwidth ( $B$ ) of our GIF can be calculated approximately by using  $B=(1/2\tau_g) = 800$  MHz.km. This result is in good qualitative agreement with other results, principally obtained by Buckler, in reference 13. However, the exact shape of the DMD signature does have profound influence on the bandwidth obtained. Apart from the maximum DMD time, what is very important is the span of mode group number  $(m/M)$  over which the DMD time remains constant. Hence Buckler<sup>13</sup> obtained a very high bandwidth of 1430 MHz.km even when the DMD time increased, from 0 to  $\approx 200$  psec/km, with  $(m/M) \approx 0,1$ , but remained constant over the much greater range  $0,1 < (m/M) < 1,0$ ; indicating equalization of propagation times over a very large portion of the graded profile. As already mentioned, knowledge of the  $a_{opt}$  value is not needed; what is important is a constant DMD time over a large  $(m/M)$  range.

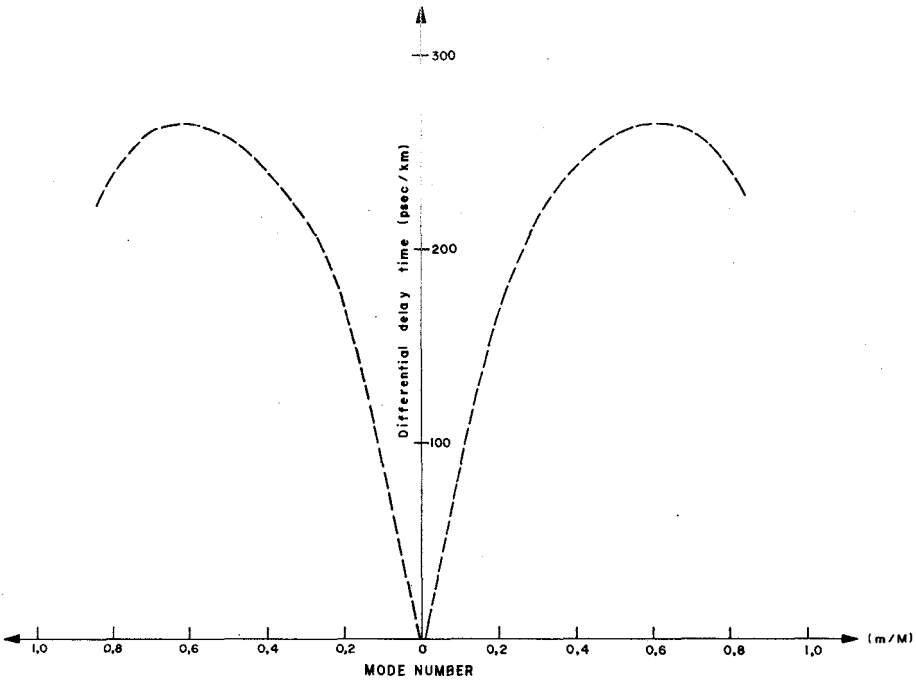


Fig.7 - The average differential delay time, from fig.6, plotted as a function of mode number  $(m/M) = (r/a)^2$ .



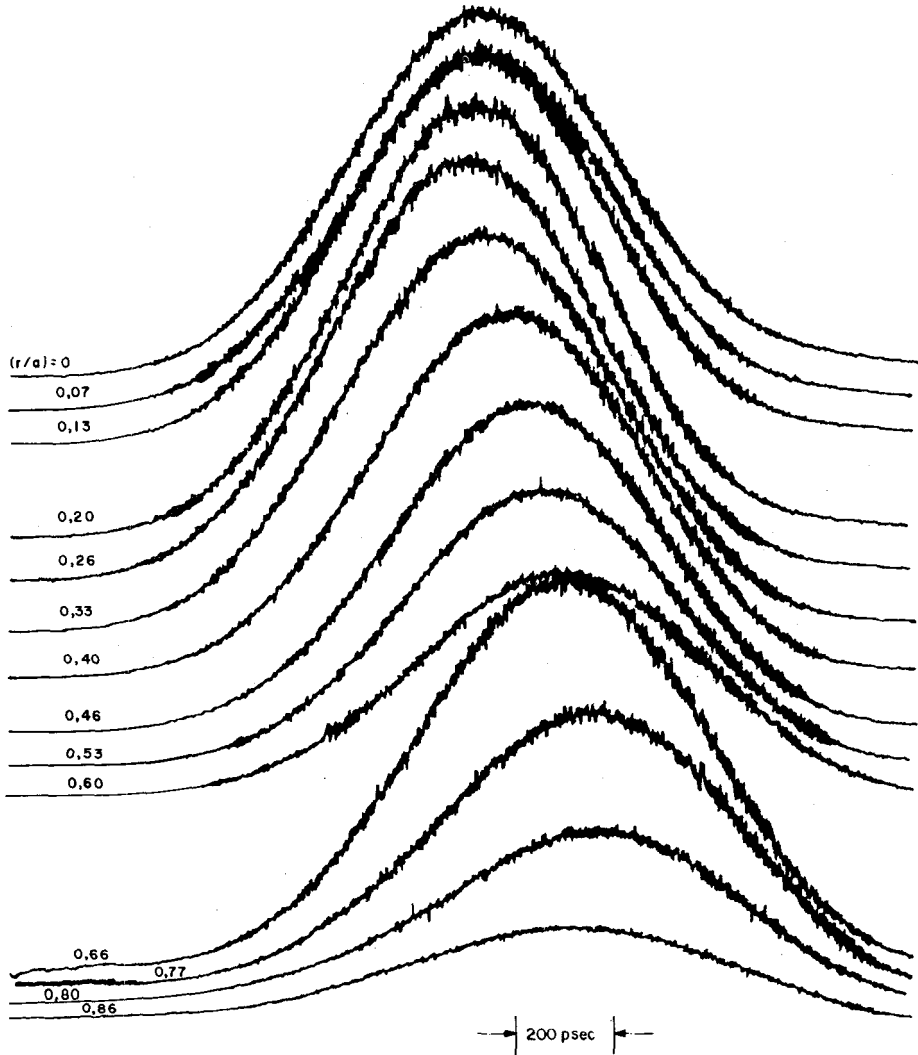


Fig.8 - Output scan obtained as a function of normalisea radial position  $(r/a)$ , as shown on the scans; mode selection at the *output* end of the fibre.

For our second series of DMD measurements, we selected a few propagating modes of the BNR fibre at the output end. All modes of the fibre were excited with a  $\times 10$  microscope objective M2, having a numerical aperture of 0,25, greater than that of the fibre (0,16). The SVF was butt-coupled to the output end of the BNR fibre and it is the first time that such an arrangement has been used. The output scans for the increasing radial positions are shown in fig. 8. As the radial position

( $r/a$ ) is increased, the pulse amplitude decreases due to differential mode attenuation, Due to this, we increased the sensitivity of the oscilloscope, for higher ( $r/a$ ) values, so as to resolve the peak of the pulse more clearly. As done previously, a similar set of scans were obtained for radial positions in the opposite direction and the results are plotted in fig. 9; also shown is the average value of the DMD time, calculated from the radial positions on either side of the core axis.

Comparing figures 6 and 9, we notice that the DMD signatures are approximately similar, i.e. the delay time increases as ( $r/a$ ) is increased with a maximum at ( $r/a$ )  $\approx 0,8$ ; hence it is at approximately this point that maximum deviation of  $a$  from  $a_{opt}$  exists. To compare these graphs more closely, we have plotted the average values, from figures 6 and 9, in fig. 10. For ( $r/a$ )  $> 0,2$ , we observe that the DMD time difference bet-

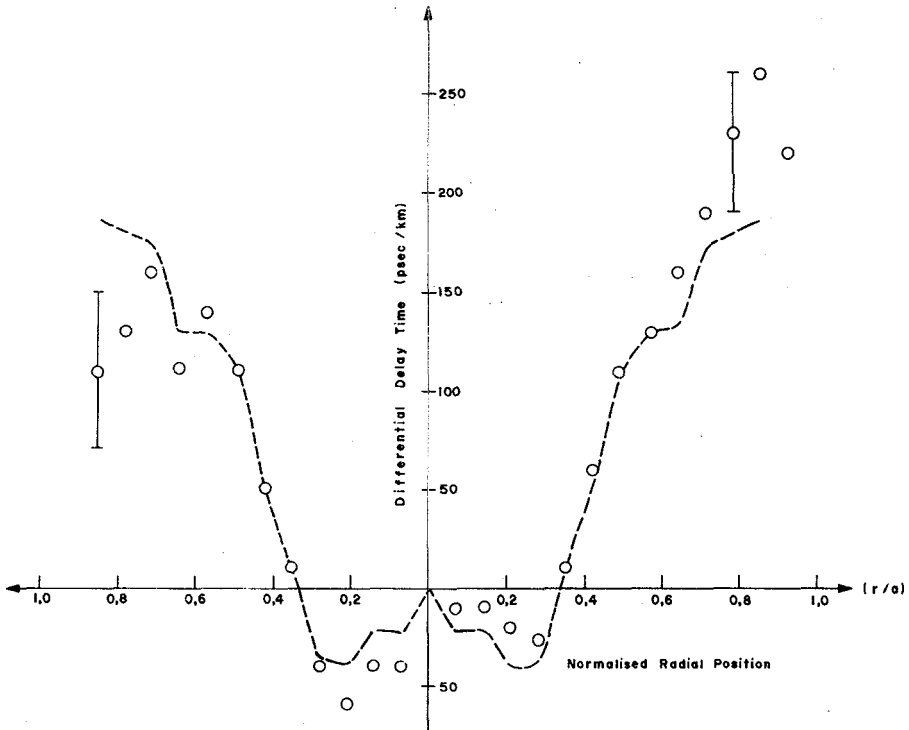


Fig.9 - Differential delay time as a function of normalised radial position ( $r/a$ ), measured at the pulse peaks, for mode selection at the output end of the fibre. The points  $\circ$  are experimentally measured points; the dashed line (-----) is the average of the experimental points on either side of ( $r/a$ ) = 0.

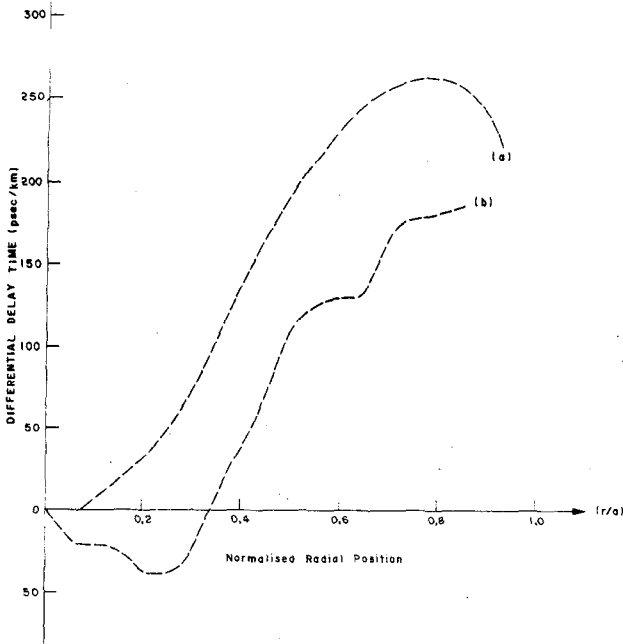


Fig.10 - Comparison of the average differential delay times obtained (a) from fig. 6; (b) from fig. 9, for mode selections at the input and output ends of the fibre respectively. Due to the symmetry, only one side is shown.

ween the two curves is approximately constant at  $\approx 80$  ps. This implies that mode conversion, although fairly small, has taken place in the fibre. We can imagine that in an absolutely perfect waveguide which was completely straight along its kilometre length, the two DMD signatures would match up exactly, since each mode would have its unique propagation angle all along the fibre length. Hence no difference would be observed by mode selection at the input end or at the output end of GIF. However, in practice the situation is quite different and mode conversion can take place due to many reasons: (i) refractive index variations in the radial direction, along the fibre due to the preform fabrication process. If this is the main cause of mode conversion in our results, the difference of  $\approx 80-100$  psec/km implies that  $n$  changes by only 0,01 from its optimum value, using the calculations made in reference 7; but this is enough to increase  $\tau$  by an order of magnitude; (ii) Our test fibre has a second coating which can cause microbending loss and mode conversion; (iii) the fibre is not straight along its kilometer length but has

bends, as it is wound on an expanded polystyrene drum with 33 cm diameter, (iv) the core diameters differ at the fibre ends, 56,6 μm compared to 61 μm. These figures were supplied by BNR and subsequently confirmed with measurements in our laboratories.

There is a second distinct difference in the two DMD signatures in fig. 10. For  $(r/a) < 0,35$ , we observe a negative DMD time with mode selection at the output end of the GIF, although this is fairly small, 40 psec. The implication is that within this region, the modes selected at the output end propagated in regions with  $\alpha > \alpha_{opt}$  and also  $\alpha < \alpha_{opt}$ , but the effect on the total propagation time was slightly dominated by  $\alpha < \alpha_{opt}$ , i.e overcompensated profile and hence negative DMD time, as discussed previously.  $\Delta t < 40$  psec implies  $\Delta n < 0,004$ , a very small index variation indeed. For  $(r/a) > 0,35$ , fibre lengths with  $\alpha < \alpha_{opt}$  would be small, as the total delay time is always positive, implying  $\alpha > \alpha_{opt}$ , i.e an undercompensated profile.

We do not observe negative DMD with selective mode excitation of the GIF, even at the first radial displacement with  $(r/a) = 0,07$ . This must be due to mode conversion, to modes with  $(r/a) > 0,35$  so that the small negative DMD time is cancelled out, with positive DMD time for these higher order modes, as already verified above. As  $(r/a)$  is increased, positive DMD time always dominates.

In order to verify the above mode conversion, we measured the full-widths, at half-maximum intensity points, of all the pulses in figs. 5 and 8 and the measured values are shown in Table 2. Although the mean values are very similar, (0,75 nsec and 0,73 nsec) the standard deviations are not (0,01 nsec and 0,05 nsec). Further, there are three distinct regions, of the radial positions, that need to be considered carefully: (i)  $0 < (r/a) < 0,35$ ; (ii)  $0,35 < (r/a) < 0,65$  (iii)  $0,65 < (r/a) < 1,0$ . This can be observed clearly from the graphical representation, of the results in Table 2, in fig. 11.

In the first region, with mode selection at the output end, curve (b), the widths are distinctly smaller than with mode selection at the input end, curve (a). This confirms mode conversion for curve (a). The negative DMD time for  $(r/a) < 0,35$  helps to reduce the width of the output pulses in this region, as shown in curve (b). This is not surprising as

TABLE 2 - Full-widths at half-maximum intensity points of the pulses obtained in figs. 5 and 8, for mode selection at the input and output ends of the graded-index fibre respectively.

Normalized radial Position ( $r/a$ )	Fig. 5 Mode Selection at input end: FWHM in nsec	Fig. 8 Mode Selection at output end: FWHM in nsec
0	0,74	0,70
0,07	0,74	0,68
0,14	0,75	0,68
0,21	0,77	0,68
0,28	0,77	0,71
0,35	0,74	0,72
0,42	0,75	0,72
0,49	0,74	0,73
0,57	0,75	0,73
0,64	0,75	0,77
0,71	0,74	0,77
0,78	0,75	0,75
0,85	0,77	0,76
0,92	0,75	0,85
Mean	0,75	0,73
Standard Deviation	0,01	0,05

most  $\text{GeO}_2\text{-SiO}_2$  fibres have a dip in the refractive index in this region, caused by the evaporation of  $\text{GeO}_2$  in the collapsing process<sup>2</sup> when making the preform rod. Unequal evaporation of the  $\text{GeO}_2$  along the preform rod can cause the refractive index differences along the subsequently pulled fibre with  $\alpha < \alpha_{\text{opt}}$  as well as  $\alpha > \alpha_{\text{opt}}$ ; however,  $\Delta\alpha$  is very small,  $< 0,004$ .

In the second region,  $0,35 < (r/a) < 0,85$ , it can be seen from fig. 11 that the widths for both selections are very similar, within the measurement accuracy. Observing the curves in fig. 10, we observe that within this region, the slopes of the delay time vs.  $(r/a)$  curves are si-

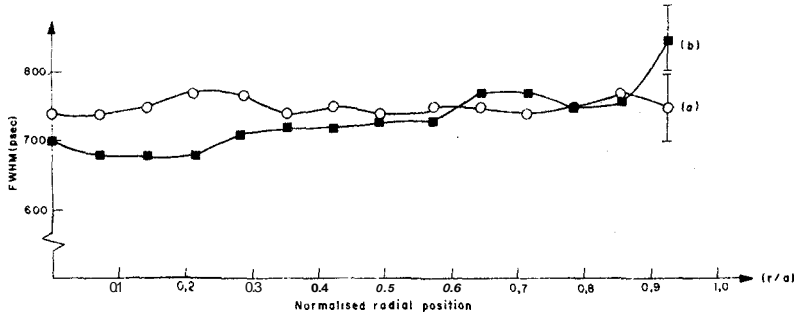


Fig. 11 - Full-widths at half-maximum intensity points, as a function of normalised radial position ( $r/a$ ), obtained (a) from fig. 5 and (b) from fig. 8, for mode selections at the input and output ends of the fibre respectively. Again, due to symmetry, only one side is shown.

milar. Hence it is to be expected that the total dispersion, as measured by the widths, also be similar. Differences in the slopes show up as slight differences in the widths, as observed by comparing figs. 10 and 11 at a particular value of ( $r/a$ ) within the region specified.

In the third region,  $0,85 > (r/a) < 1,0$ , we have only slight differences in the widths for both mode selections as seen again in fig. 11. However, contrary to the results for the first region specified above, now the widths, with mode selection at the output end, are slightly greater than those with mode selection at the input end; but the results are within the measurement accuracy as shown with the error bars. This arises due to the small amplitude of the pulses near ( $r/a$ ) - 1.

We shall now discuss the utmost importance of DMD measurements in graded-index multimode fibres linked together in a long communications link, especially the length dependence of intermodal dispersion ( $\tau_g$ ). If a fibre has *complete* mode mixing, or intermodal coupling, the DMD time will be constant and independent of the radial launching position, as the complete coupling will force all modes to have an average propagation time through the length of the fibre. In this case,  $\tau_g$  will be reduced and further, increase as the square-root of the fibre length; but some additional loss, in addition to the scattering and absorption loss of the fibre, will occur as coupling will also take place to radiation modes. Due to this square-root length dependence of  $\tau_g$ , the bandwidth of such fibres interconnected together will improve significantly.

Otherwise, if a fibre has a *negligible* amount of intermodal

coupling, DMD time will be zero for all radial positions only if the profile is optimum. However, this  $a_{opt}$  is fairly difficult to achieve as shown by DMD measurements and small changes in  $a$  can have a marked effect on  $\tau_g$ . However, if the DMD time can be held constant, at any value but preferably small, over a large region of radial positions,  $\tau_g$  can be reduced, and the bandwidth can be increased considerably as clearly shown by Buckler<sup>13</sup>. In this case such fibres, with negligible intermodal coupling, linked together will show a linear dependence of dispersion, as long as the DMD signatures of all the fibres in the link have either positive or negative delay. Hence in very long links, many tens of kilometers, it can be seen that mode-coupled fibres will have a greater bandwidth than non-mode-coupled fibres, but at a loss penalty, as already discussed above. But the overriding and decisive advantage in non-mode-coupled fibres is that positive DMD time, for undercompensated profiles, and negative DMD time for overcompensated profiles simply add arithmetically, as shown again by Buckler<sup>14</sup>. Physically, this can be understood by considering one ray, which has its unique propagation path through the fibres and will travel at different velocities in different fibres depending on the local refractive index. This will be true also for all other rays as well, with the effect that all rays will have the same total propagation time through all the fibres linked together, if the arithmetic sum of the DMD times at each value of radial position is zero. Hence multimode graded-index fibres having non-optimum  $a$  values can have zero total dispersion, when linked together, by (i) operating in the  $1.3 \mu\text{m}$  region for zero material dispersion, (ii) linking non-mode-coupled fibres, have positive and negative DMD time, so that their summation at each  $(r/a)$  position, is zero. However, this latter requirement would be difficult to achieve in practice. Nevertheless, with a DMD signature of each fibre, selection of fibres can be made to give a nearly constant DMD time, not necessarily zero, at each  $(r/a)$  position, hence optimising the bandwidth of these fibres linked together, by reducing the value  $\tau_g$ . It is not necessary to worry about optimum refractive index profiles in fibres. Non-optimum fibres produced while optimising  $\alpha$  using DMD measurements, can still be used as long as the intermodal coupling is negligible. The measurements we have demonstrated in this paper can be used to probe in detail the propagation in the fibre, especially the intermodal coupling.

## 5. CONCLUSIONS

We have made DMD measurements in a graded-index fibre using a single-mode fibre and for the first time, carried out selection of a few guided modes of the fibre *both* at its input and output ends. By doing so, we have probed mode coupling effects in the fibre with a fairly simple experimental system. DMD measurements are of utmost importance in a graded-index multimode fibre as they give a direct indication of the deviation of the refractive index profile from its optimum value and are to be preferred over direct measurements using interferometric techniques. Further, these DMD measurements can be used to improve the bandwidth of subsequently pulled fibres, and hence can be used on a quality control basis in a production environment.

We thank Telecomunicações Brasileiras S/A (TELEBRÁS), for financially supporting the work and fibres used in the delay line; F.P.Kapron, of Bell Northern Research, Canada, for kindly supplying the graded-index Fibre used; M.G.Destro and Harlete A. Zamprônio for assisting with some measurements. One of us (S.M.S.) thanks the University of Maringá, Paraná, for leave of absence and a post-graduate scholarship.

## REFERENCES

1. H.R.D.Sunak and J.B.M.Ayres Neto, "Intermodal Pulse dispersion in multimode optical fibres and its measurement with a Nanosecond Test Facility", *Revista Brasileira de Física*, 10(3), 499-515, (September 1980).
2. S.E.Miller and A.G. Chynoweth (Eds.) *Optical Fibre Telecommunications*, Academic Press (1979).
3. R.Olshansky and D.B. Keck, "Pulse broadening in graded-index optical fibres", *Appl. Optics*, 15, 483-491 (1976).
4. D.Gloge and E.A. J. Marcattili, "Multimode Theory of graded core fibers", *Bell System Technical Journal*, 52, 1563-1577, (1973).
5. L.G.Cohen, "Pulse Transmission measurements for determining near optimal profile gradings in multimode borosilicate optical fibres", *Applied Optics*, 15(7), 1808-1814 (July 1976).



6. L.Jeunhomme and J.P.Pacholle, "Selective mode excitation of graded-index optical fibres", *Applied Optics*, 17(3), 463-468 (February 1978).
7. R.Olshansky and S.M.Oaks, "Differential Mode Delay Measurement", *Proceedings of the Fourth European Conference on Optical Communication, Genova, 1978*, p. 128-132.
8. L.Jeunhomme, J.P.Pacholle, and J.Raffy, "Wavelength dependence of modal dispersion in graded-index optical fibres", *Electronics Letters*, 14(12), 364-366, (8th June 1978).
9. G.Cancellieri, "Time Dispersion measurement in optical fibre by near- and far field scanning technique", *Electronic Letters*, 14(15), 465-467, (20th July 1978).
10. B.Costa, F.Esposto and B.Sordo, "Wavelength dependence of differential group delay in graded-index optical fibres: application to fiber-links characterization", *Proceedings of Optical Fiber Communications Conference, Washington, 1979*, pp. 122-125.
11. L.Jeunhomme and P.Lamouler, "Intermodal dispersion measurements and interpretation in graded-index optical fibres", *Optical and Quantum Electronics*, 12, 57-64 (1980).
12. M.J.Buckler, "Differential Group Delay measurement using single-mode fibre selective excitation", *Proceeding of Conference on Precision Electromagnetic Measurements, Braunschweig, 1980*, pp. 224-227.
13. M.J.Buckler, J.W.Shiever and F.P.Partus, "Optimization of Multimode fibre bandwidth via differential group delay Analysis" *Proceedings of the Sixth European Conference on Optical Communication, York, U.K., 1980*, pp. 33-36.
14. M.J.Buckler, "Optimization of concatenated fibre bandwidth via differential Mode delay", *NBS Special Publication n° 597*, pp. 59-62, 1980, with proceedings of Symposium on Optical Fibre Measurements.
15. H.R.D. Sunak and J.B.M. Ayres Neto, "Material Dispersion Measurements in optical fibre waveguides", *Revista Brasileira de Física*, 10(3), 445-456, (1980).